Land subsidence and hydrodynamic compaction of sedimentary basins

H. Kooi, J. J. de Vries

Hydrology and Earth System Sciences, 2(2–3), *159–171* (1998) © EGS

Hydrology & Earth System Sciences

Land subsidence and hydrodynamic compaction of sedimentary basins

H. Kooi and J.J. de Vries

Faculty of Earth Sciences, Vrije Universiteit, De Boelelaan 1085, 1081 HV, Amsterdam
Email kooi@geo.vu.nl

Abstract

A one-dimensional model is used to investigate the relationship between land subsidence and compaction of basin sediments in response to sediment loading. Analysis of the model equations and numerical experiments demonstrate quasi-linear systems behaviour and show that rates of land subsidence due to compaction: (i) can attain a significant fraction (>40%) of the long-term sedimentation rate; (ii) are hydrodynamically delayed with respect to sediment loading. The delay is controlled by a compaction response time τc that can reach values of 10^5–10^7 yr for thick shale sequences. Both the behaviour of single sediment layers and multiple-layer systems are analysed. Subsequently the model is applied to the coastal area of the Netherlands to illustrate that lateral variability in compaction-derived land subsidence in sedimentary basins largely reflects the spatial variability in both sediment loading and compaction response time. Typical rates of compaction-derived subsidence predicted by the model are of the order of 0.1 mm/yr but may reach values in excess of 1 mm/yr under favourable conditions.

Introduction

Land subsidence causes problems in the sustainable development of low lying coastal regions such as deltas which house a significant part of the human population (Barends *et al.*, 1995). Together with the potential rise in sea level due to greenhouse warming, land subsidence contributes to loss of fertile land and fresh water reserves. At present, changes in ocean water volume seem to be the primary concern of policy makers but, in most impact assessments, the contribution of land subsidence, albeit not investigated, is at least recognized (e.g., Eisma, 1995).

Land subsidence occurs in many parts of the world as a natural phenomenon, as a result of human activities, or both (Barends *et al.*, 1995). Anthropogenic causes of land subsidence include withdrawal of fluids, such as groundwater, geothermal fluids, oil and gas, and extraction of solids during mining and tunnelling activities. At present, most studies of land subsidence have focused on these anthropogenic effects. This is reflected in the proceedings volumes of the five international symposia on land subsidence, published by the IAHS as Publications no. 88–89, 121, 151, 200 and 234. Examples of natural causes of land surface movement include glacio- and hydro-isostasy, tectonic activity, natural compaction, and the development of sinkholes due to solution processes. Natural vertical land movements are important because they form the long-term background for evaluating the more recent anthropogenic factor in land subsidence and sea level change.

The present paper examines land subsidence resulting from natural hydrodynamic compaction of clastic basin sediments in response to sediment loading. Firstly, some approaches to compaction modelling are discussed. Then, a numerical model of vertical compaction and fluid flow is presented which can handle arbitrary sediment loading histories and where newly deposited sediments become part of the model. Next, the compaction time scale of a single sediment layer is derived and the associated compaction behaviour discussed and illustrated with numerical model experiments. Subsequently, multiple layer systems are analysed in a similar way. The analyses illustrate that land subsidence rates due to compaction of clastic units can reach values that are comparable with current glacio- and hydro-isostatic subsidence rates. Furthermore, this subsidence is very persistent and can continue far into the future, even when sedimentation ceases.

These concepts and results are illustrated in an application of the numerical model to The Netherlands coastal area. Predictions of current land subsidence in map view are presented for two sets of model assumptions and their differences interpreted in terms of compaction response times.

Finally, the implications of the results are discussed with reference to studies of relative sea-level change, the

delta cycle and geodetic measurements of land subsidence.

It should be stressed that it is not the aim of this paper to present a numerical model containing novel features; the model employed is basically a one dimensional version of existing compaction-fluid flow models (e.g., Bethke, 1985; Ungerer *et al.*, 1990; Audet and McConnell, 1992). The prime aim of the present paper is to use these models to demonstrate the importance of natural hydrodynamic compaction of sedimentary basins for land subsidence studies and to establish, for the first time, an approximate relationship between compaction-derived subsidence of the land surface/sea bottom and sedimentation rate for variable sediment loading.

Approaches to compaction modelling

The problem of land subsidence by natural compaction bears many similarities to the geotechnical phenonemon of settlement, following the emplacement of a construction. Settlement problems are generally restricted to static loading where the load is of limited size, while sedimentation entails gradual long-term dynamical loading which is relatively uniform over large areas (Gibson, 1958). Irrespective of the specific problem, compaction models should include conservation and constitutive equations for both the fluid and solid phase. The two phases are coupled through the state of stress.

Fluid flow in porous media is commonly considered to be governed by Darcy's law, $q_{fl} = -(k/\mu).(\nabla p_{fl} - \rho_{fl} g)$, where q_{fl} is the Darcy fluid velocity, k the permeability tensor, μ, p_{fl}, and ρ_{fl} denote the viscosity, pressure and density of the fluid, respectively, and g is gravitational acceleration. Neuzil (1986) notes that the broad acceptance of Darcy's law may not be tenable under all conditions because Darcy's law remains essentially untested for low-permeability environments. Only for flow of high-salinity brines have deviations from Darcy's law been demonstrated unequivocally (Hassanizadeh and Leijnse, 1988).

Constitutive relationships for the solid phase are less clear and depend, amongst others, on sediment type, and temperature and pressure conditions. In soil mechanics, Terzaghi's effective stress, $\sigma_{eff} = \sigma - p_{fl}$ (total stress minus pore pressure) is commonly combined with a compressibility modulus of the sediments. Compressibility is commonly characterized by a compression index, C_c, which relates the change in void ratio, e, linearly to the change in the logarithm of effective stress (Sanglerat *et al.*, 1984). Modelling hydrodynamical consolidation using this approach entails the calculation of the temporal evolution of effective stress, for example, after a construction is put in place, or in response to groundwater extraction (e.g., Leake, 1991). C_c is obtained from oedometer tests of sediment samples (Skempton, 1944) and accounts for primary consolidation. Secondary consolidation or secular strain of clay and peat results from gradual adjustments of the skeleton structure at constant effective stress, and can be described as a visco-elastic creep process (e.g., Den Haan and Edil, 1994). Creep may be responsible for observations that compressibilities derived from porosity-depth relationships in sedimentary sequences tend to be higher than compressibilities obtained from laboratory measurements at short time scales (e.g., Neuzil, 1986). Yet, still other studies (e.g., Audet, 1996) find that no such discrepancy exists for shales of the Louisiana Shelf in the Gulf of Mexico. Miao and Wu (1991) find that accounting for secondary consolidation improves predictions of land subsidence due to pumping at a time scale in the order of 100 days. At time scales of several years and longer, secondary compaction probably becomes insignificant. Biogenic processes often further complicate the compaction process at shallow levels and at short time scales (Deverel, and Rojstaczer, 1996).

Whether the concepts of soil mechanics are also valid for compaction at basin scale and at geological timescales is questionable. Many studies of sedimentary rocks at depths below one kilometre indicate that chemical compaction processes such as pressure solution are the dominant cause of porosity reduction of carbonates and quartz-rich sediments (e.g., Houseknecht, 1987). Pressure solution is governed by a viscous constitutive relationship (Angevine and Turcotte, 1983; Rutter, 1983). However, the effective viscosity of sedimentary rock is little constrained and the process only partly understood (e.g., Dewers and Hajash, 1995).

In spite of the above uncertainties and complexities, the principles of soil mechanics are used successfully in models of fluid flow and fluid pressure history of sedimentary basins at geological time scales and at spatial scales of many kilometres, both in horizontal and vertical directions (e.g., Bethke, 1985; Van Balen and Cloetingh, 1993; Audet and McConnell, 1994; Kooi, 1997, and many older works referenced therein). In these models, sediment compressibility is commonly derived from empirical porosity-depth relationships (Hermanrud, 1993). Although future studies may lead to more appropriate formulations of compaction models of deep basin sediments (e.g., Schneider *et al.*, 1996), in the following, the conventional principles of soil mechanics will be used—that is, Darcy's law, Terzaghi's principle of effective stress, and long-term porosity-effective stress relationships—to infer what these assumptions imply regarding the role of compaction of deep basin sediments in land subsidence.

Model description

The model calculates one-dimensional, vertical compaction, fluid flow and fluid pressure evolution of a sediment column during and following deposition. Model equations are written in terms of excess fluid pressure

$p_{ex} = p_{fl} - p_h$ in which p_{fl} is total fluid pressure and

$$p_h = \int_{surf}^{z} (\rho_{fl} g h) dh$$

the hydrostatic pressure exerted by the overlying water column. In the model, compaction is driven by the vertical component of effective stress, $\sigma_{eff,z} = \sigma_z - p_{fl}$. It is assumed that the total vertical stress is given by the lithostatic pressure (overburden)

$$\sigma_z = \int_{surf}^{z} (\rho_b g h) dh$$

in which ρ_b denotes bulk density. Because the model is one-dimensional, in the following the subscript z will be dropped.

Combining Darcy's law and Terzaghi's effective stress with mass conservation, assuming incompressible grain material and a fully saturated sediment column, the following expression for excess fluid pressure can be derived in a reference frame attached to the grain material (Kooi, 1997)

$$(\phi\beta_{fl} + \beta_p)\frac{\partial p_{ex}}{\partial t} = \nabla \cdot \left(\frac{k}{\mu}\nabla p_{ex}\right) + \beta_p(\rho_{gr} - \rho_{fl})g v_{gr} - \phi\beta_{fl}\rho_{fl} g v_z \quad (1)$$

In equation (1), ϕ is porosity; β_{fl} and β_p are the fluid and drained pore compressibility, respectively, defined by $\beta_{fl} = -(1/V_{fl}).(\partial V_{fl}/\partial P_{fl})$ and $\beta_p = -(1/V_b).(\partial V_{fl}/\partial \sigma_{eff})$, where V_b and V_{fl} denote bulk volume and pore volume, respectively. Because incompressible grain material is assumed, β_p is equivalent to bulk (total) compressibility. Further, ρ_{gr} and v_{gr} are the density and sedimentation rate of the grain material (positive for deposition), respectively. v_{gr} is evaluated for zero porosity. v_z is the subsidence rate of the rock relative to water table or sea level (positive for growing distance). This term arises because a Lagrangian reference frame is used. Equation 1 shows how a temporal change of overpressure is the result of competition between diffusional dissipation (first term right hand side) and source terms (combined second and third term right hand side). The vertical strain rate of the sediments (negative for contractional strain) is given by

$$\frac{\partial \varepsilon}{\partial t} = \frac{1}{(1-\phi)}\frac{\partial \phi}{\partial t} = -\beta_p \frac{\partial \sigma_{eff}}{\partial t} \quad (2)$$

The rate of land subsidence due to compaction follows from integration of Eqn. 2 over the total height of the sediment column.

One-dimensional finite elements with linear shape functions are used for p_{ex} (Istok, 1989). The elements are coupled to the rock matrix and are advected relative to the fluid during compaction. Each element is assigned one lithology. Each lithology is characterized by: (i) ρ_{gr}; (ii) $\phi = \phi_o exp(-b.\sigma_{eff})$; and (iii) $k = k_r.10^{-c1+\phi c2}$. From (ii) it follows that $\beta_p = b\phi/(1-\phi)$. (iii) is an empirical relationship which has been used in several studies (e.g., Bethke, 1985; Mello *et al.*, 1994). The relationship yields an unrealistic finite permeability for zero porosity. However, it describes permeability adequately for the range of porosity values which occur in model experiments. A split-node technique for the porosity field allows porosity to be discontinuous across element boundaries when the lithology of neighbouring elements is different. Problems are solved by implicit finite differencing in time with Picard iterations to account for nonlinearities in average porosity of the elements, $\bar{\phi}$, k and β_p. New elements are added to the top of the growing sediment column in the model during deposition. For further details of the integration of the model equations, the reader is referred to Kooi (1997). In the present model, erosion is not considered.

Parameter values which are kept constant in all of the model experiments presented in this paper are listed in Table 1. Because values of shale permeability reported in the literature vary greatly, two sets of parameter values are given for shale, nominally referred to as high and low permeabilities respectively. The high permeability relationship corresponds to measurements reported by Neglia (1979). The low permeability relationship was adopted from Bryant *et al.* (1975) based on measurements on Gulf Coast shale. These two relationships are used to illustrate the influence of permeability on model behaviour. The behaviour for still other permeability estimates, such as for low values recently reported by Neuzil (1994), can be understood readily from the present analysis and does not impair the message of this paper.

Table 1. Parameter values

	$c1$ (–)	$c2$ (–)	ϕ_o (–)	b (Pa^{-1})	ρ_{gr} ($kg \cdot m^{-3}$)
shale (low k)	21.0	6.0	0.5	$5.0 \cdot 10^{-8}$	$2.72 \cdot 10^3$
shale (high k)	20.0	8.0	0.6	$5.0 \cdot 10^{-8}$	$2.72 \cdot 10^3$
sand	13.4	2.0	0.5	$2.5 \cdot 10^{-8}$	$2.65 \cdot 10^3$

$\mu = 5 \cdot 10^{-4}\ Pa \cdot s$
$\beta_{fl} = 4.3 \cdot 10^{-10}\ Pa^{-1}$
$\rho_{fl} = 1000\ kg \cdot m^{-3}$
$g = 9.8\ m \cdot s^{-2}$
$k_r = 1\ m^2$

Analysis of model compaction behaviour

COMPACTION OF A SINGLE SEDIMENT LAYER

Figure 1 shows results of a numerical model experiment in which a shale layer of thickness L=200 m with initial hydrostatic fluid pressure is buried by sand at a uniform sedimentation rate v_s = 1 mm yr^{-1}. The rate of compaction, $v_c = ds/dt$, of the shale layer (Fig. 1c) grows in an exponential-like fashion towards a steady-state which

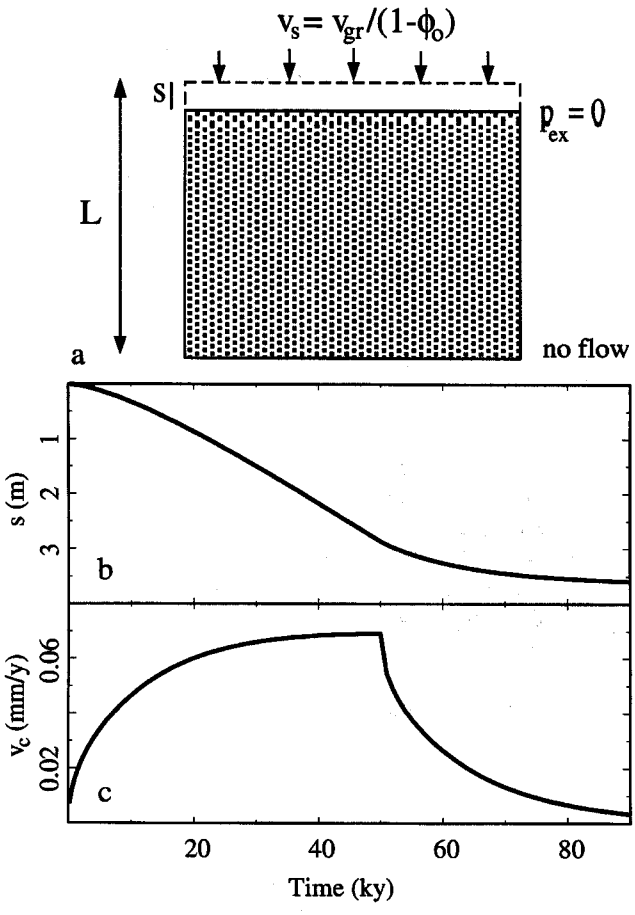

Fig. 1. *Numerical experiment of compaction of a single shale layer under sediment loading. (a) General configuration of experiments involving a single sediment layer as discussed in the main text and definition of variables. (b,c) Model predictions for L = 200 m, v_s = 1 mm/yr, loading material = sand, and the parameter values of Table 1 for low shale permeability. Sediment loading ceases at 50 ky. (b) Compaction of shale layer. (c) Rate of compaction shale layer.*

amounts to approximately $0.07.v_s$. When sedimentation suddenly ceases at 50 kyr, v_c decays in a similar exponential way to zero. This behaviour is reminiscent of a linear system where v_s is input and v_c output.

In Appendix A, an analytical expression of this exponential-like response to a step change in sedimentation rate is derived from the model equations assuming (initially) that β_p and hydraulic diffusivity $D_h = k/(\mu(\phi\beta_f + \beta_p))$ are constant for the compacting layer. The derived expression is of the form

$$v_c(t) = Ae^{-t/\tau_c} + F.v_s \qquad (3)$$

where F, the ratio of compaction to sedimentation rate in steady state ($t = \infty$), is given by

$$F = \beta_p L(\rho_{gr} - \rho_f)g(1 - \phi_o) \qquad (4)$$

and A is a constant.

The compaction time scale τ_c for a single sediment layer subject to a hydrostatic top and no-flow bottom boundary condition as in the experiment of Fig. 1, is given by

$$\tau_c = \frac{4L^2}{\pi^2 D_h}. \qquad (5)$$

The factor $4/\pi^2$ is not essential, but is retained in τ_c to comply with the conventional meaning of the response time of a linear system in the sense that, for a step change in forcing, the system has covered a fraction $(1 - 1/e)$ of the total distance toward the new steady state after a time $t = \tau_c$.

It is instructive to note that F (Eqn. 4) depends on compressibility and sediment thickness and does not depend on permeability. Values of β_p derived from porosity depth relationships range typically from $> 10^{-7}$ Pa^{-1} in the first hundreds of metres from the surface to 10^{-8} Pa^{-1} at 1 km depth to $< 10^{-9}$ Pa^{-1} at depths larger than 5 km (e.g., Hermanrud, 1993; Neuzil, 1986, Fig. 4). Inserting $\beta_p = 5.10^{-8}$ Pa^{-1}, $g = 10$ m.s^{-2}, $(\rho_{gr} - \rho_f) = 1700$ kg.m^{-3}, and $\phi_o = 0.5$ in eqn. (4) gives $F = 4.25.10^{-4}L$, which shows that when thick, highly compressible basin units L~10^3 m are involved at relatively shallow depth, the rate of compaction-derived subsidence can potentially attain a significant fraction of the sedimentation rate. F is obviously dominated by the more compressible sediments in the top few kilometres and does not increase dramatically when deeper basin sediments are considered. These aspects are fully accounted for in the numerical modelling presented further on (e.g., Figs. 3 and 4 for lower shale compressibilities).

Significance of the compaction time scale

Apart from the factor $4/\pi^2$, the compaction time scale is equivalent to the well known consolidation time scale (Terzaghi and Peck, 1949; Domenico and Schwartz, 1991). However, the compaction time scale, as used here, is assigned a more general meaning. While the consolidation time scale refers to the amount of vertical shortening after a load is emplaced instantaneously, τ_c characterizes the adjustment of the *rate* of vertical shortening in response to the *rate* of sediment loading.

The inferred exponential approach of a new steady state compaction rate (Eqn. 3; Fig. 2a) implies that the compaction rate evolves at a rate proportional to the disequilibrium compaction rate. That is,

$$\frac{\partial v_c}{\partial t} \approx (v_c^s - v_c)/\tau_c \qquad (6)$$

in which $v_c^s = F.v_s$. Equation 6 describes the behaviour of a Kelvin visco-elastic body with Young's modulus $E = 1/\beta_p$ and viscosity $\eta = \tau_c/2\beta_p$ (Fig. 2a). The behaviour of Eqn. 6 for any temporal sedimentation history is

well known from linear systems analysis and can be described by a transfer function which characterizes the amplitude and phase response in the Fourier domain (for details one is referred to a relevant text book on linear systems). Figures 2b,c,d illustrate three characteristic regimes in the compaction behaviour. (1) When the sedimentation rate varies slowly with period $t_p >> \tau_c$ (Fig. 2b), then the actual compaction rate at any instant will be close to equilibrium (steady state) for the current sedimentation rate. In other words, the compacting layer has enough time to adjust to the changes in loading. (2) Conversely, when the sedimentation rate contains very rapid variations with period $t_p << \tau_c$ (Fig. 2c), the compaction rate will not be able to adjust to these short-term variations, and the actual compaction rate will largely reflect the long-term average sedimentation rate. That is, short-term variations are nearly completely damped. The associated phase shift, or delay of about $t_p/4$ in the response is, therefore, not of great importance. (3) For intermediate variations in sedimentation rate with period $t_p \approx 2\pi\tau_c$ (Fig. 2d), the compaction rate is attenuated with respect to the equilibrium compaction rate v_c^s by approximately a factor of 2 and is delayed by approximately $t_p/8$.

Thus, τ_c is useful as a measure of the response of the compacting layer to variations in sedimentation rate and in identifying those phases in the history of sediment loading that contribute significantly to the current compaction rate. For instance, sediment loading that took place more than three times τ_c ago and variations in sedimentation rate with periods $t_p << \tau_c$ can be largely ignored. τ_c also provides a measure of how long compaction will continue into the future in the absence of further loading.

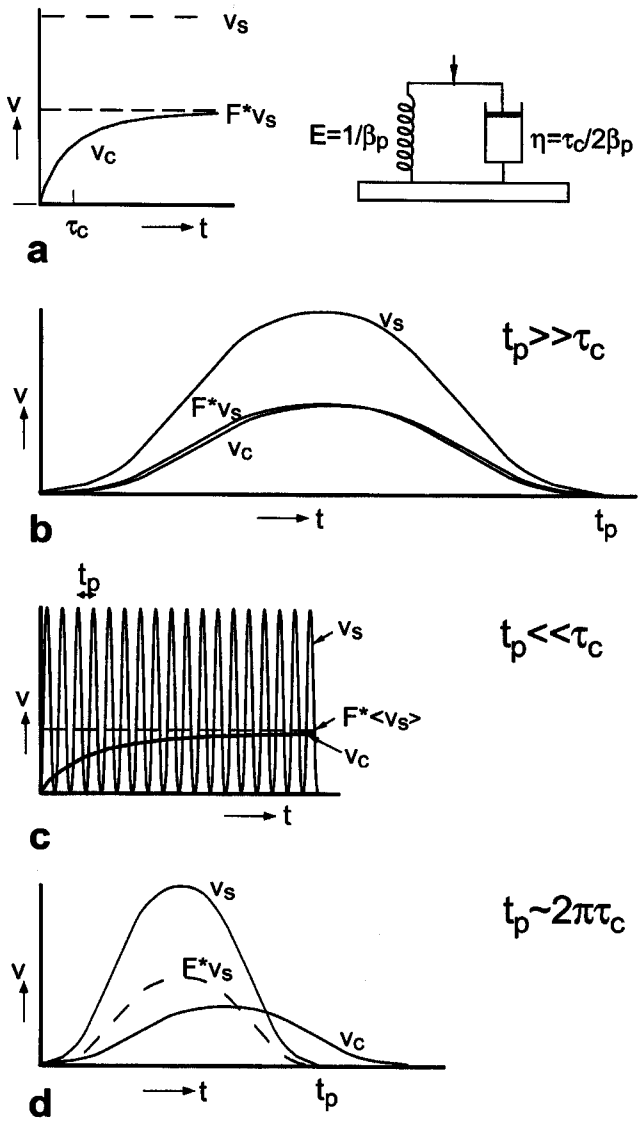

Fig. 2. *Cartoon illustrating the compaction behaviour of a single sediment layer for various loading conditions. (a) Left: exponential approach to steady state of the compaction rate v_c for a step change in sedimentation rate v_s. Right: Kelvin visco-elastic body gives same response. Variations in sedimentation rate relative to τ_c are (b) slow; (c) rapid; (d) intermediate. A more detailed discussion is given in the text.*

TYPICAL VALUES OF τ_C, F, V_C, AND DEVIATIONS FROM LINEAR BEHAVIOUR

τ_c only gives an approximate characterization of the compaction response of a sediment layer. Deviations from the exponential response to a step change in sedimentation rate are caused by contributions from higher harmonics in the initial disequilibrium pressure distribution ($n>0$ in Appendix A) and, more importantly, temporal variations in D_h, β_p and L during compaction. Nonlinearity caused by spatial variation of D_h, β_p is generally relatively small as will be shown in the next section.

Nonlinearity is small when $\tau_c v_s << L$, because then the shale layer will experience little compaction during the exponential approach to steady state. This is generally true for shales with relatively high permeability (Fig. 3). The converse is true when $\tau_c v_s \sim L$, which tends to occur for thick, low-permeability shales (Fig. 4). Compaction rates in Figs. 3 and 4 increase with the thickness of the shale layer. F reaches 40% for the 1 km thick shale in Fig. 3.

In spite of the non-linearity observed in Fig. 4, rough estimates of τ_c can still be made and used to characterize the compaction response, if only in a semi-quantitative way. τ_c can easily amount to 10^5 yr for a 1000 m thick shale. Time scales > 10^7 yr can be reached for sedimentary basins with sediment piles in excess of 10 km (Kooi, 1997).

Typical values of v_c can be estimated from $v_c = F.v_s$ where v_s is a typical sedimentation rate at time scale τ_c. At a time span $\tau_c = 10^3$ yr, typical sedimentation rates are 1 mm yr^{-1}, but may be as high as 100 mm yr^{-1} (Sadler, 1981). Using $F = 0.2$ gives rates of land subsidence in the range 0.2–20 mm yr^{-1}. At a time span $\tau_c = 10^7$ yr, corresponding to a thick, very low-permeability substrate,

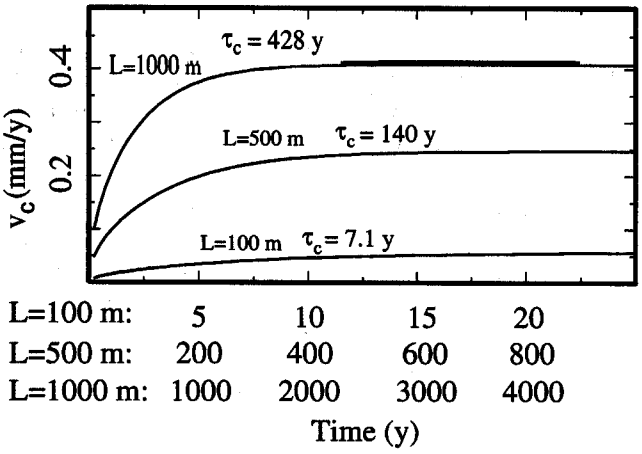

Fig. 3. *Almost perfect exponential response of v_c to step change in sediment loading for shale layer thicknesses L=100 m, L=500 m and L=1000 demonstrates linear compaction behaviour for the high shale permeability estimates (Table 1). Estimates of τ_c are given. Loading with sand with v_s = 1 mm/yr.*

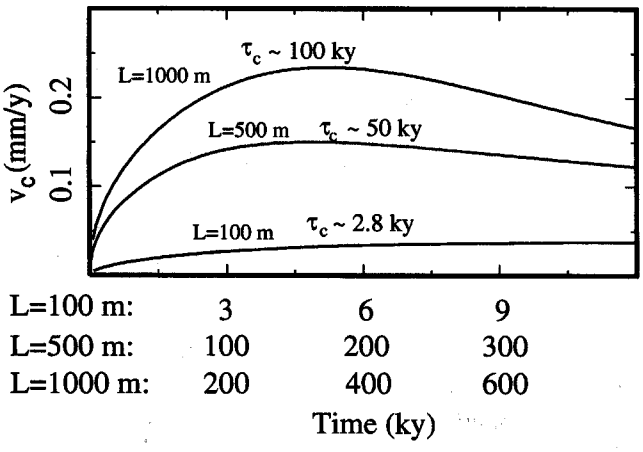

Fig. 4. *Same as Fig. 3 for low shale permeabilities (Table 1). Non-linear behaviour reflected in deviations from exponential response. Approximate values of τ_c for the phase in which v_c increases are shown.*

v_s = 0.01 mm yr^{-1}, but may reach 1 mm yr^{-1} (Sadler, 1981), giving land subsidence rates of 0.002–0.2 mm yr^{-1}. These figures are borne out by the numerical model.

RESPONSE OF A LAYERED SYSTEM

Vertical flow

When D_h and β_p vary strongly in the vertical, for instance in a sand-shale sequence, analytical approximations such as those derived in Appendix A are not obtained readily. However, numerical model experiments show that, even under these conditions, the system response is approximately linear. This is illustrated by the exponential nature of the dashed curve in Fig. 5b which was obtained by assigning b=10^{-10}*Pa*$^{-1}$ for the sands in the sequence shown in Fig. 5c to produce strong contrasts in both quantities. The linear behaviour may seem counterintuitive. However, it reflects the fact that, for vertical flow, the evolution of excess pressures and hence, compaction of individual layers of a sand-shale sequence are fully coupled to that of the other layers in the sequence. In Appendix A, this is shown in mathematical terms in Eqn. A13.

For the special case where a single thick, high permeability compartment is overlain by a thin, low permeability seal, an expression for the compaction response time was recently presented by Kooi (1997).

Lateral flow

The discussion so far has dealt with vertical flow only. Yet, in sand-shale sequences, lateral flow in the sand layers is often prominent. In the case of very efficient lateral drainage, the sand layers will maintain close-to hydrostatic pore pressures while flow in the shales is near vertical. Under those circumstances, the response times of the individual shale layers (with hydrostatic top and bottom boundary conditions) are 4 times smaller than for a no-flow bottom boundary condition

$$\tau_c = \tau_0 = \frac{L^2}{\pi^2 D_h}. \qquad (7)$$

The response of the system as a whole is then simply the sum of the responses of the individual layers. Figure 5 illustrates this behaviour in a numerical model experiment. The instantaneous response of the sand layers, the rapid response of the thin shale layer, and the slow response of the thick shale layer can be distinguished clearly in the compaction history (Fig. 5a,b). The different response times of the various layers are also reflected in the excess pressure evolution (Fig. 5c).

The instantaneous reaction of the sand layers in the above model to mimic laterally unconfined conditions is a rough approximation (end-member situation). The delay in compaction response of these sand layers can become quite significant when the lateral drainage distance is large. The detailed behaviour due to lateral flow, including propagation of compaction from the lateral boundaries towards the centre of the aquifer, requires two- or three-dimensional flow models. However, some rough response characteristics can be constructed from Eqn. 7 where L should be replaced by the lateral drainage distance of the aquifer, W. The resulting compaction time scale is for one-dimensional flow and pertains to the average compaction along the aquifer. It shows that the response time of the sand layer becomes significant relative to that of a shale layer when $W^2/D_h^{sand} \oplus L^2/D_h^{shale}$. For two-dimensional radial flow, the square dependence of W becomes a linear dependence.

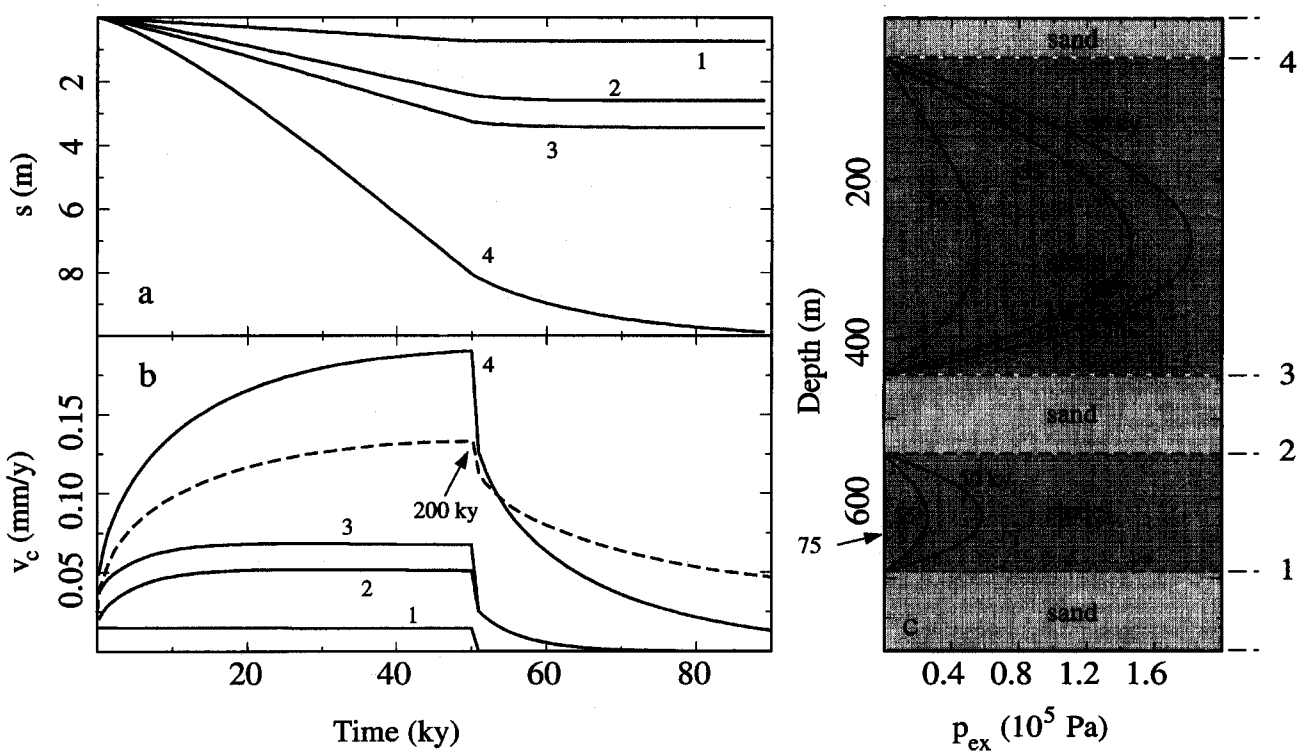

Fig. 5. *Results for layered sand-shale sequence with one thick (400 m) and one thin (150 m) shale layer, separated by laterally unconfined sand layers (c). Loading as for Fig. 1. Dashed curve in (b): experiment adopting vertical flow in the entire sequence and compressibility parameter* $b = 10^{-10} Pa^{-1}$ *for the sands to illustrate quasi-linear behaviour also applies when* β_p *and k vary strongly with depth. Note that for this experiment the time scale on the horizontal axis should be multiplied by a factor 4. Continuous curves: Efficient lateral flow in sand layers modelled by imposing hydrostatic fluid pressures. (a) Subsidence relative to the base of the sediment column for the four numbered horizons in (c). (b) Rate of subsidence for the horizons. (c) Decay of overpressures following the end of sedimentation at 50 ky.*

Illustrative example for the western part of The Netherlands

The analysis presented in this paper has shown that basin thickness and its compressibility (Eqn. 4), the compaction response time (Eqn. 5) and the history of sediment loading are the main controls of current compaction-derived land subsidence predicted by the adopted model. In sedimentary basins, all of these controls can vary strongly laterally. In this section, the importance of lateral variations in these quantities is illustrated for the western part of the Netherlands using two numerical model experiments. It should be noted that the experiments are not meant to provide a validation of the model; that issue will be addressed in the discussion section. The regional application serves to illustrate the role of lateral variations in the above mentioned parameters in a generic sense.

In the models, the following assumptions are made: (a) vertical flow, (b) no compaction of pre-Tertiary basin units (no flow boundary condition for base Tertiary) and (c) sediment properties according to Table 1. None of these assumptions may be tenable in the face of detailed observational data and will be modified in a more detailed regional study of land subsidence in the Netherlands (to be published later). However, the assumptions illustrate the above relationships.

The grid chosen covers the provinces of Noord- and Zuid Holland and part of the province of Zeeland (Fig. 6d) with a resolution of 10 km. Sediment thickness data (Fig. 6a–c) were obtained from depth-contour maps (R.G.D., 1985; Van Doorn *et al.*, 1985; Geluk and Wildenborg, 1988). Tertiairy and early Pleistocene deposits in the study area consist largely of marine shales and reach thicknesses in excess of 1000 m in the Voorne Trough and IJsselmeer region in the SW and NE of the study area, respectively (Fig. 6c). The subsequent fluvial Pleistocene sediments increase in thickness from south to north in the study area (Fig. 6b). Holocene sediments contain significant amounts of clay and peat. Maximum thicknesses of some 25 m occur at two loci along the coast and decrease rapidly in thickness towards the east (Fig. 6a).

Shale, sand and shale lithologies were adopted for the Tertiary, Quaternary and Holocene units, respectively. Hydrostatic fluid pressures are assumed for the end of the Tertiary. For each grid point, the local Pleistocene column is deposited at a uniform rate over a period of 2 Myr;

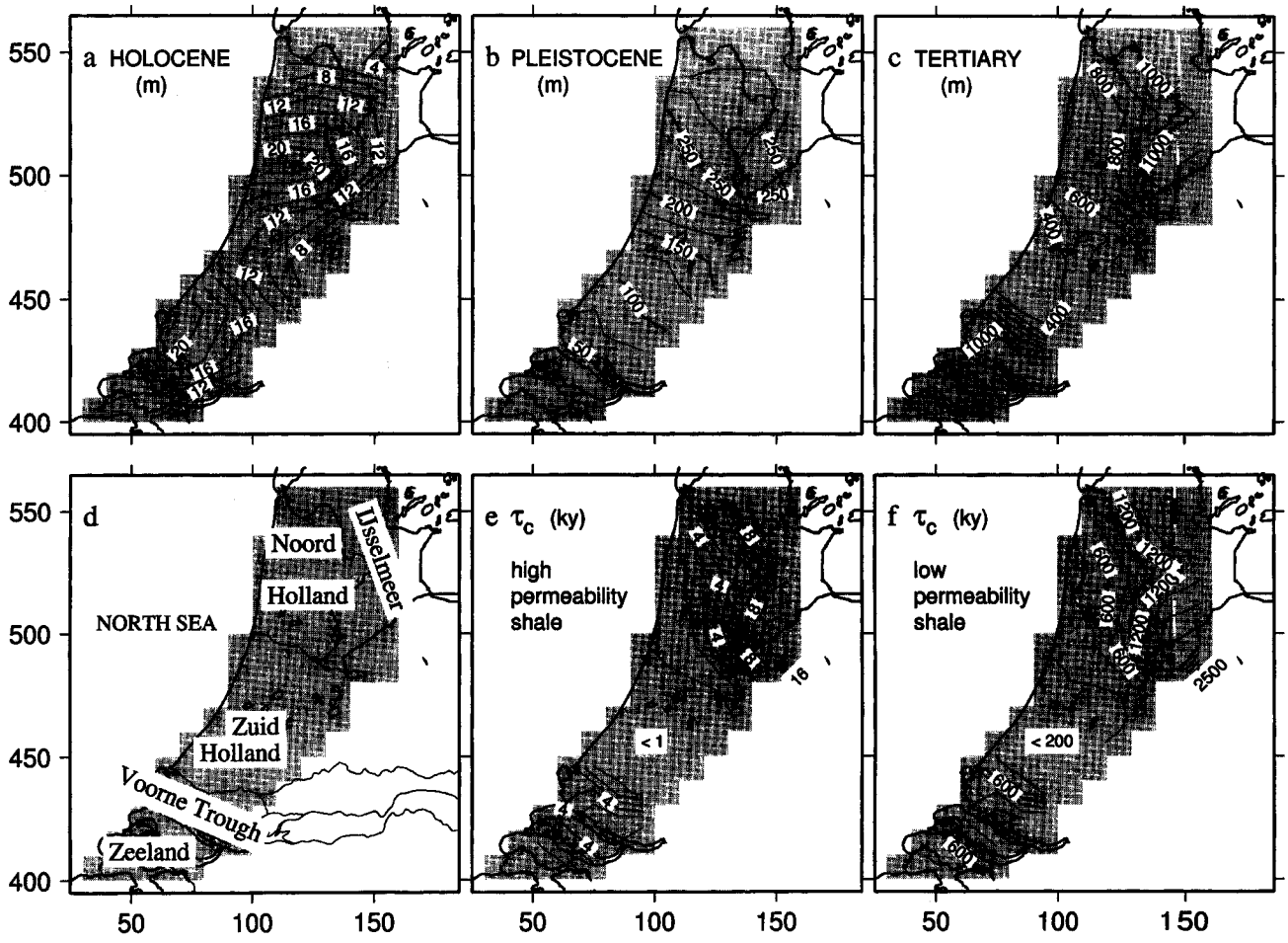

Fig. 6. *Stratigraphic data used in the regional modelling study of the western part of the Netherlands. Shading denotes the study area. Labelling according to the standard Dutch stereographic projection (RD) coordinate system in km. (a) Depth to base Holocene. (b) Thickness fluvial Pleistocene. (c) Thickness Tertiairy, including marine Pleistocene. (d) Names of provinces and other regions referred to in the text. (e) Estimated compaction response times of Tertiary; high permeability shales. (f) As (e) for low permeability shales.*

Holocene is deposited according to relative sea-level rise along the central Dutch coast (R.G.D., 1985) with high sedimentation rates of 10 mm yr^{-1} during the early Holocene, gradually decreasing to the present (inset Fig. 7a).

Figure 6e,f displays the compaction response time of the Tertiary shales in plan view for both the high and low estimates of shale permeability (Table 1). τ_c was calculated from Eqn. 5 where D_h was evaluated using average values of β_p, ϕ and k for the Tertiary shale column at its present burial depth, assuming normal compaction (hydrostatic fluid pressures). Response times for high shale permeability (Fig. 6e) range from 5 ky in the SE to 16 ky in the IJsselmeer region. In Zuid Holland, τ_c is of the order of 1 ky. These values suggest that current compaction rates are sensitive to Holocene, and in particular late Holocene sedimentation rates. For low permeability estimates (Fig. 6f), τ_c reaches values in excess of 1 Myr in the Voorne Trough and up to 2.5 Myr in the IJsselmeer region, while in Zuid Holland τ_c is still higher than 0.1 Myr. For these conditions, current compaction rates are affected not only by Holocene sediment loading, but also by late Pleistocene sedimentation.

Figure 7 displays the predicted rate of land subsidence due to compaction of Tertiairy and younger sediments in plan view for both the high and low permeability estimates of shale. Rates are of the order of 0.1 mm yr^{-1} in both cases. For high permeability shales (Fig. 7a), the distribution of subsidence is influenced strongly by the spatial differences in thickness of the Tertiary shales. This is expected, because predictions are dominated by late Holocene sedimentation rates, which are rather uniform over the entire area. By contrast, for low permeability shales (Fig. 7b) the predicted subsidence pattern shows a much stronger correlation with the map of Holocene sediment thickness (Fig. 6a). Apparently, the very high early Holocene sedimentation rates (10 mm yr^{-1}), which occurred only where the present Holocene is thicker than

some 15 m, exert a strong control on predicted compaction rates in this case.

The predicted rates of compaction-derived subsidence of the order of 0.1 mm yr^{-1} represent a significant contribution to total land subsidence of 0.1 to 0.6 mm yr^{-1} inferred from long-term geodetic levelling data in the present study area (Lorenz *et al.*, 1995). It is interesting to note that the pattern of differential subsidence of Fig. 7b is in excellent agreement with the map of land subsidence reported in the latter study.

Discussion and conclusions

In this paper, a model based on conventional principles used in modelling of compaction and fluid flow in sedimentary basins—that is, Darcy's law, Terzaghi's principle of effective stress and long-term porosity-effective stress relationships—has been used to study the implications of these assumptions for the contribution of compaction of deep basin sediments to land subsidence. As discussed in the section 'Approaches to compaction modelling' the validity of all of these assumptions can be questioned. Of the assumptions, the use of porosity-effective stress relationships derived from porosity-depth data is probably the most problematic because these relationships describe sediment compressibility at time scales of the order of 10^5 yr and up. These long-term compressibilities may contain contributions by visco-elastic creep processes. Unfortunately, the time scales on which such creep processes operate are basically unknown. However, if creep strain rates become negligible at time scales of, say, several tens of years, predictions of the model are quite accurate because current compaction rates would be dictated by the rate at which pore fluids can be expelled rather than by creep rates. Only when the visco-elastic time scale is of the same order or larger than the hydrodynamic time scale of the compaction response time (Eqn. 5) would it affect the model behaviour significantly. Therefore, using long-term compressibilities inferred from porosity-depth data is reasonable, in particular when thick (> 100 m), low-permeability basin units are involved.

The behaviour of the present model suggests that natural compaction of basin sediments plays an important role in current and future land subsidence, in particular in deltaic settings with high long-term sedimentation rates. Rates of subsidence due to compaction can reach a significant fraction of the sedimentation rate when thick basin units are involved. Hydrodynamic delay in the compaction response, which can be expressed in terms of a compaction response time, can attain values of the order of 10^5–10^7 yr depending mainly on the lithological architecture and associated permeability distribution in the subsurface. As a result, sediment loading that occurred many hundreds of thousands or several millions of years ago may affect current compaction.

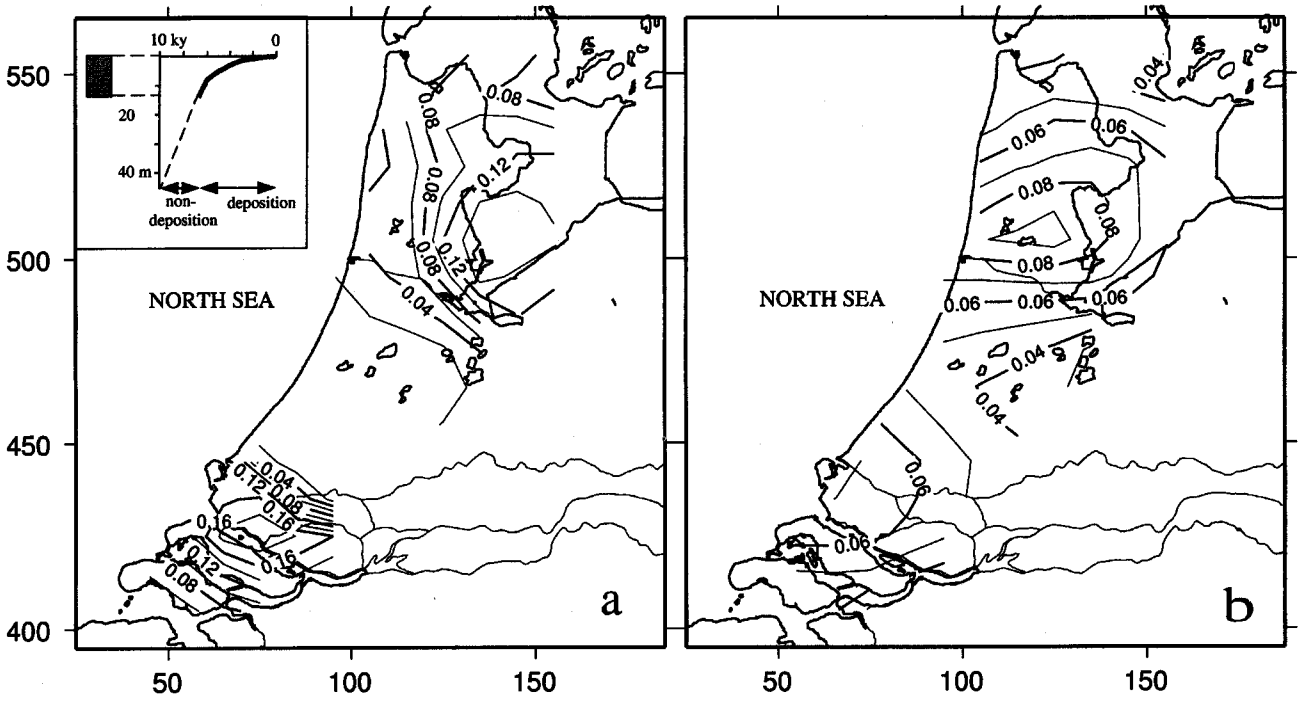

Fig. 7. *Calculated current rate of land subsidence due to compaction of Tertiairy and younger sediments (in mm/yr) in the study area. (a) High permeability shales. (b) Low permeability shales. Inset in (a) shows how Holocene sedimentation rates in the model are controlled by the relative sea-level rise (dashed curve) along the Dutch coast. Shaded area to the left denotes a 14 m thick Holocene sediment column.*

Modelling suggests that typical rates of compaction are of the order of 0.1 mm yr^{-1} but may reach values > 1 mm yr^{-1} in some areas. These rates are of the same order as those caused by glacio- and hydro-isostasy away from the major Weichselian continental ice sheets (Lambeck and Johnston, 1995). Compaction of the deep subsurface may therefore be responsible for relatively high rates of sea-level rise inferred from tide-gauge records in several deltas across the globe (Emery and Aubrey, 1991). Basin compaction may also be an important player in drowning of coastal wetlands following delta-lobe abandonment such as in the Mississippi delta (Coleman and Roberts, 1991; Kuecher, 1995).

Large uncertainties in detailed model predictions for regional studies arise from (a) limited control on the (large-scale) permeabilities of deep basin sediments, in particular shales (Neuzil, 1986), and; (b) lack of knowledge of the role of chemical diagenesis and compaction processes in the deeper parts of sedimentary basins. Therefore, the model predictions would gain in credence if they could be supported by direct observations of short-term compaction rates within the sedimentary column. Unfortunately, direct measurement of average strain rates of the order of 10^{-7} yr^{-1}, for instance in observation wells, is probably intractable. Consequently, constraints on model behaviour will have to come from indirect observations.

At present, three types of indirect constraints are considered to be potentially useful: (a) recent land subsidence rates from geodetics (and tide-gauge records); (b) measurements of fluid overpressures in the subsurface; and (c) regional comparison of Holocene relative sea-level curves. Recent land subsidence rates do not reflect only compaction, but also include contributions from isostasy and tectonic deformation within the crust and, sometimes, within the sedimentary basin itself. Removing the latter components is not a trivial task. In particular, prediction of tectonic rates at short time scales is highly problematic. Moreover, both tectonic and compaction-derived subsidence are likely to correlate with the same underlying basin structure, inhibiting discrimination of the two components based on wavelength considerations.

When sediment loading is the only source of fluid overpressure generation, overpressures are a direct measure of undercompaction and hence, ongoing compaction. When overpressures are known throughout the column, compaction rates can be inferred provided the permeabilities of the sediments are accurately known. The latter provides a problem. Moreover, overpressure data at intermediate depths are neither of interest to ground water exploration nor to the hydrocarbon industry and are, therefore, difficult to obtain.

Differential compaction of pre-Holocene strata could be reflected in regional differences of Holocene relative sea-level curves inferred from the sedimentary record. However, differential compaction of 0.1 mm yr^{-1} would correspond to 0.5 m difference in those curves over 5,000 yr, a value which is of the same order as the error bars assigned to relative sea-level curves in the Netherlands (e.g., Van der Plassche, 1995); probably the best studied area in the world. Moreover, effects of tectonics, local tidal climate and to a lesser extent, isostasy, would have to be known accurately. Therefore, inferences concerning compaction using this source of information would be, at best, only tentative.

The authors feel that the physical principles underlying the current model are sufficiently sound to believe that its behaviour and model predictions regarding land subsidence are meaningful. The lack of unequivocal observational constraints for the model implies the advisability of a large number of regional studies in areas where at least a number of the above indirect constraints are available. The first of these regional studies will focus on the Dutch delta.

Appendix A

The exponential-like response to step changes in sediment loading revealed by the experiment of Fig. 1 can be understood from the following analysis which, in the absence of sedimentation, is similar to classical consolidation theory (Terzaghi and Peck, 1949). This analysis differs from that of Gibson (1958) in that consideration is given, not to a sediment column growing in time from zero thickness, but to the consolidation of a pre-existing sediment layer decreasing in thickness upon burial by younger deposits and its contribution to land subsidence (total land subsidence would also include the compaction within the overlying growing sediment column). Furthermore, arbitrary sediment loading histories are also considered.

In the following, firstly an approximate analytical solution to the problem of Fig. 1 is derived assuming both the hydraulic diffusivity $D_h = k/(\mu(\phi\beta_{fl} + \beta_p))$ and compressibility β_p of the shale layer are uniform, and constant with time (they are not constant in Fig. 1). Subsequently it is shown that the linear behaviour does not depend on the constancy of D_h and β_p, but that quasi-linear behaviour also occurs when hydraulic properties vary strongly in the vertical.

Vertically constant D_h and β_p

When the total strain of the layer is small such that L can be taken as constant, excess fluid pressure distribution evolves toward a steady state (Fig. A1) given by the solution of

$$D_h \frac{\partial^2 p_{ex}^S}{\partial z^2} = C = [\phi\beta_{fl}\rho_{fl} g v_z - \beta_p(\rho_{gr} - \rho_{fl}) g v_{gr}]/(\phi\beta_{fl} + \beta_p) \quad \text{(A1)}$$

where C is a constant. For boundary conditions, ($p_{ex}(z = 0) = 0$) and ($\partial p_{ex}/\partial z(z = L) = 0$) (note that z=0 refers to

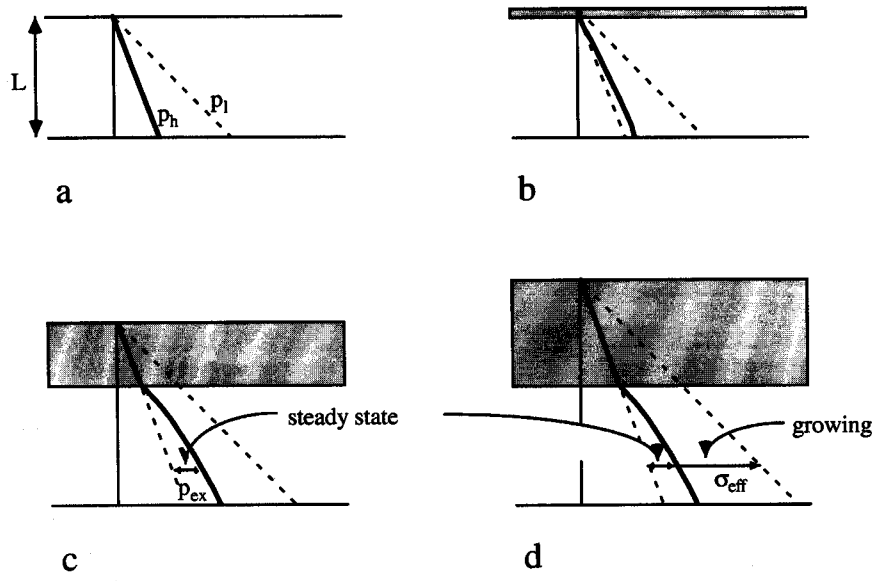

Fig. A1. *Cartoon illustrating the evolution of the various pressure components in a sediment layer that is buried at a constant rate by high permeability sediment. A no-flow basal boundary condition is assumed. (a) Initial, hydrostatic fluid pressures. (b) Build up of excess fluid pressure in the early stage of sediment loading. (c,d) Excess fluid pressure distribution achieves a (near) steady state while effective stress keeps on growing at a rate proportional to the sedimentation rate.*

the top of the layer that is being buried, not to the land surface),

$$p_{ex}^S = \frac{C}{D_h}(\tfrac{1}{2}z^2 - Lz). \qquad \text{(A2)}$$

The excess fluid pressure at any time is the sum of the steady state and a transient component

$$p_{ex} = p_{ex}^S + p_{ex}^T \qquad \text{(A3)}$$

where the transient component obeys

$$\frac{\partial p_{ex}^T}{\partial t} = D_h \frac{\partial^2 p_{ex}^T}{\partial z^2} \qquad \text{(A4)}$$

with initial condition $p_{ex}^T\ (t = 0) = p_{ex}\ (t = 0) - p_{ex}^S$. The solution of this classical diffusion problem for the above boundary conditions can be written as an infinite series of exponentially decaying harmonics (Carslaw and Jaeger, 1959)

$$p_{ex}^T(z,t) = \sum_{n=0}^{\infty} a_n\, e^{-t/\tau_n} \cdot \cos\left[\frac{(2n+1)\pi z}{2L}\right] \qquad \text{(A5)}$$

where a_n follows from harmonic decomposition of p_{ex}^T $(t = 0)$, and where

$$\tau_n = \frac{4L^2}{D_h(2n+1)^2\pi^2} \qquad \text{(A6)}$$

Equations A5 and A6 show that the higher harmonics for initial condition $p_{ex}^T(z,\ t = 0)$ disappear first, leaving the fundamental $(n = 0)$ whose amplitude decays exponentially with decay time τ_0.

The next step in the analysis of the compaction behaviour is to recognize that the vertical strain rate (Eqn. 2) can be decomposed into contributions by sedimentation rate and the rate of change of excess pressure.

$$\frac{\partial \varepsilon}{\partial t} = -\beta_p \frac{\partial[\sigma - p_h - p_{ex}]}{\partial t} = \beta_p \frac{\partial p_{ex}}{\partial t} - \beta_p(\rho_{gr} - \rho_{fl})g v_{gr} \qquad \text{(A7)}$$

in which the right-hand side follows from substituting $\partial\sigma/\partial t = \rho_{fl} g v_z + (\rho_{gr} - \rho_{fl})g v_{gr}$ and $\partial p_h/\partial t = \rho_{fl} g v_z$. The strain rate of the entire layer is obtained by integration (note that ρ_{gr} and v_{gr} are constant over the layer because they refer to the sediment load, not to the compacting column).

$$\frac{1}{L}\int_0^L \frac{\partial \varepsilon}{\partial t} dl = -\frac{v_c}{L} = \beta_p \frac{\partial \langle p_{ex}\rangle}{\partial t} - \beta_p(\rho_{gr} - \rho_{fl})g v_{gr} \qquad \text{(A8)}$$

In Eqn. A8, average excess pressure $\langle p_{ex}\rangle$ can be replaced by the transient component $\langle p_{ex}^T\rangle$ because $\langle p_{ex}^S\rangle$ does not contribute to the time derivative. Using Eqn. A5, one obtains

$$\langle p_{ex}\rangle = \langle p_{ex}^T\rangle = \sum_{n=0}^{\infty} a_n \frac{2(-1)^n}{(2n+1)\pi} e^{-1/\tau_n} \qquad \text{(A9)}$$

Substitution in Eqn. A8 and rearranging yields an expression for the compaction rate

$$v_c(t) = \frac{\beta_p D_h}{2L}\left[\sum_{n=0}^{\infty} a_n(-1)^n(2n+1)\pi \cdot e^{-t/\tau_n}\right] + \beta_p L(\rho_{gr} - \rho_{fl})g v_{gr} \qquad \text{(A10)}$$

in which the first and second terms on the right hand side are the transient and steady state compaction rates, v_c^T and

v_c^S, respectively. Equation A10 shows that in the very first phase $t \oplus 0$, higher harmonics provide important contributions to v_c^T. However, their contribution disappears rapidly. For instance, at $t = \tau_0$, the relative magnitude of the n=1 and n=0 harmonics is given by $v_{c,n=1}^T / v_{c,n=0}^T \oplus -10^{-3}(a_1/a_0)$. Hence, to a first approximation

$$v_c(t) = \frac{a_0 \pi \beta_p D_h}{2L} e^{-t/\tau_0} + \beta_p L(\rho_{gr} - \rho_{fl}) g v_{gr} \quad \text{(A11)}$$

In steady state, the ratio of compaction rate to sedimentation rate is

$$F = \frac{v_c^S}{v_s} = \beta_p L g(\rho_{gr} - \rho_{fl})(1 - \phi_0) \quad \text{(A12)}$$

Variable β_p in the vertical

Inserting a non-constant value of β_p in Eqn. A8 gives

$$-\frac{v_c}{L} = \beta_p^* \frac{\partial \langle p_{ex} \rangle}{\partial t} - \langle \beta_p \rangle (\rho_{gr} - \rho_{fl}) g v_{gr} \quad \text{(A13)}$$

where $\beta_p^* = \frac{1}{L} \int_0^L \beta_p \frac{\partial p_{ex}}{\partial t} \mathrm{dl} \Big/ \frac{\partial \langle p_{ex} \rangle}{\partial t}$

is the average β_p for the layer using the weighting function $w(z,t) = \partial p_{ex} / \partial t$. β_p^* = const. not only when β_p = const., but also when $w(z,t)$, or the normalized weighting function $w(z,t)/\langle w \rangle$ are a function of z only (time independent). The latter condition implies $w(z,t) = F(z)*G(t)$. This is approximately true for a layered system in which flow occurs in the vertical only and reflects the fact that excess pressures in the layers evolve in concert (the shape of excess pressure distribution with depth is approximately constant). Despite the nicks that will occur typically in $p_{ex}(z)$, $\langle p_{ex} \rangle$ and $\partial \langle p_{ex} \rangle / \partial t$ will tend to approach a (approximately) steady state in an exponential-like fashion. Hence, the linear behaviour of the model is also retained when compressibility is a strong function of depth.

Acknowledgments

The research presented in this paper was partly supported by the Survey Department of the Ministry of Transport, Public Works and Water Management (Rijkswaterstaat) of the Netherlands. This is a contribution to the NEESDI (Netherlands Environmental Earth System Dynamics Initiative) programme, funded by the Netherlands Organization for Scientific Research (NWO-grant 750.296.01).

References

Angevine, C.L. and Turcotte, D.L., 1983. Porosity reduction by pressure solution, *Geol. Soc. Am. Bull.*, **94**, 1129–1134.

Audet, D.M. and McConnell, J.D.C., 1992. Forward modelling of porosity and pore pressure evolution in sedimentary basins, *Basin Res.*, **4**, 147–162.

Audet, D.M., 1996. Compaction and overpressuring in the Pleistocene sediments on the Louisiana Shelf, Gulf of Mexico, *Mar. Petr. Geol.*, **13**, 467–474.

Barends, F.B.J., Brouwer, F.J.J. and Schroder, F.H., 1995. *Land subsidence, natural causes, measuring techniques, the Groningen gasfields*, IAHS Publ. No. 234, 409 pp.

Bethke, C.M., 1985. A numerical model of compaction-driven groundwater flow and heat transfer and its application to the paleohydrology of intracratonic sedimentary basins, *J. Geophys. Res.*, **90**, 6817–6828,

Bryant, W.R., Hottman, W. and Trabaut, P., 1975.Permeability of unconsolidated marine sediments, Gulf of Mexico, *Mar. Geotechnol.*, **1**, 1–14.

Carslaw, H.S. and Jaeger, J.C., 1959. *Conduction of heat in solids*, 510 pp., Oxford University Press, London.

Coleman, J.M. and Roberts, H.H., 1991. *Coastal depositional systems in the northern Gulf of Mexico, Program and Abstracts*, Gulf Coast Section, SEPM, Twelfth Research Conference, 62–64.

Den Haan, E.J. and Edil, T.B., 1994. Secondary and tertiary compression of peat. in *Proc. Int. Workshop Advances in Understanding and Modelling the Mechanical Behaviour of Peat*, Delft, June 1993, Balkema, Rotterdam, 49–60.

Deverel, S.T. and Rojstaczer, S., 1996. Subsidence of agricultural lands in the Sacramento-San Joaquin Delta, California: Role of aqueous and gaseous carbon fluxes, *Wat. Resour. Res.*, **32**, 2359–2367.

Dewers, T. and Hajash, A., 1995. Rate laws for water-assisted compaction and stress-induced water-rock interaction in sandstones, *J. Geophys. Res.*, **100**, 13,093–13,112,

Domenico, P.A. and Schwartz, F.W., 1991. *Physical and chemical hydrogeology*, 824 pp., Wiley, New York.

Eisma, D., 1995. *Climate change, impact on coastal habitation*, Lewis Publishers, Boca Raton.

Emery, K.O. and Aubrey, D.G., 1991. *Sea levels, land levels, and tide gauges*, 237 pp., Springer, New York.

Geluk, M.C. and Wildenborg, A.F.B., 1988. Geologische inventarisatie en onstaansgeschiedenis van zoutvoorkomens in noord- en oost-Nederland, *Rep.Rijks Geologische Dienst, 10568*, Haarlem, the Netherlands.

Gibson, R.E., 1958. The progress of consolidation in a clay layer increasing in thickness with time, *Geotechnique*, **8**, 171–182.

Hassanizadeh, S.M. and Leijnse, T., 1988. On the modeling of brine transport in porous media,*Wat. Resour. Res.*, **24**, 321–330.

Hermanrud, C., 1993. Basin modelling techniques—an overview, in *Basin modelling: advances and applications*, NPF Spec. Publ., 3, Elsevier, Amsterdam, pp. 1–34.

Houseknecht, D.W., 1987. Intergranular pressure solution in four quantzose sandstones, *J. Sed. Petr.*, **58**, 228–246.

Istok, J., 1989. *Groundwater modeling by the finite element method*, 495 pp., Wat. Resour. Monogr. 13, Am. Geoph. Un.

Kooi, H., 1997. Insufficiency of compaction disequilibrium as the sole cause of high pore fluid pressures in pre-Cenozoic sediments, *Basin Res.*, **9**, 227–241.

Kuecher, G.J., 1995. The dominant processes responsible for subsidence of coastal wetlands in South Louisiana, in *Land Subsidence*, edited by F.B.J. Barends, F.J.J. Brouwer, and F.H. Schroder, IAHS Publ. No. 234, 69–81.

Lambeck, K. and Johnston, P., 1995.Land subsidence and sea-level change: Contributions from the melting of the last great ice sheets and the isostatic adjustment of the Earth, in *Land Subsidence*, ed. by F.B.J. Barends, F.J.J. Brouwer, and F.H. Schroder, IAHS Publ. No. 234, 3–18.

Leake, S.A., 1991. Simulation of vertical compaction in models of regional ground-water flow, in *Land subsidence*, edited by A.I. Johnson, IAHS Publication No. 200, pp. 565–574.

Lorenz, G.K., van Beusekom, W., Groenewoud, W. and Hofman, M., 1995. Geodetic determination of land subsidence in The Netherlands, in *Land Subsidence*, edited by F.B.J. Barends, F.J.J. Brouwer, and F.H. Schroder, IAHS Publ. No. 234, 187–196.

Mello, U.T., Karner, G.D. and Anderson, R.N., 1994. A physical explanation for the positioning of the depth to the top of overpressure in shale-dominated sequences in the Gulf Coast basin, United States, *J. Geophys. Res.*, **99**, 2775–2789.

Miao, J.F. and Wu, L.G., 1991. Mathematical modelling of land subsidence due to pumping of a multi-aquifer system with viscoelastic properties, in *Land subsidence*, edited by A.I. Johnson, IAHS Publication No. 200, pp. 593–601.

Neglia, S., 1979. Migration of fluids in sedimentary basins, *Am. Assoc. Petr. Geol. Bull.*, **63**, 573–579.

Neuzil, C.E., 1986. Groundwater flow in low-permeability environments, *Wat. Resour. Res.*, **22**, 1163–1195.

Neuzil, C.E., 1994. How permeable are clays and shales? *Wat. Resour.Res.*, 30, 145–150.

R.G.D., 1985. *Atlas van Nederland, deel 13, geologie*, 23 pp., Stichting Wetenschappelijke Atlas van Nederland, Staatsuitgeverij, Den Haag.

Rutter, E.H., 1983. Pressure solution in nature, theory and experiment, *J. Geol. Soc. Lond.*, **140**, 725–740.

Sadler, P.M., 1981. Sediment accumulation rates and the completeness of stratigraphic sections, *J. Geol.*, **89**, 569–584.

Sanglerat, G., Olivari, G. and Cambou, B., 1984. *Practical problems in soil mechanics and foundation engineering, 1, Developments in geotechnical engineering Vol 34a*, pp. 283, Elsevier, Amsterdam.

Schneider, F., Potdevin, J.L. Wolf, S. and Faille, I., 1996. Mechanical and chemical compaction models for sedimentary basin simulators, *Tectonophysics*, **26**, 307–317.

Terzaghi, K. and Peck, R.B., 1949. *Soil mechanics in engineering practice*, 566 pp., Wiley, New York, 3rd edition.

Ungerer, P., Burrus, J., Doligez, B., Chenet, P.Y. and Bessis, F., 1990. Basin evaluation by integrated two-dimensional modeling of heat transfer, fluid flow, hydrocarbon generation and migration, *Am. Assoc. Petr. Geol. Bull.*, **74**, 309–335.

Van Balen, R.T. and Cloetingh, S.A.P.L. 1993. Stress-induced fluid flow in rifted basins, in *Am. Assoc. Petr. Geol., Studies in geology, 36*, edited by A.D. Horbury and A.G. Robinson, 87–98.

Van der Plassche, 1995. Evolution of the intra-coastal tidal range in the Rhine-Meuse delta and Flevo Lagoon, 5700–3000 yrs cal B.C., *Mar. Geol.*, **124**, 113–128.

Van Doorn, Th. H.M., Leyzers Vis, C.I., Salomons, N., van Dalfsen, W., Speelman, H. and Zijl, W., 1985. Aardwarmtewinning en grootschalige warmteopslag in tertiaire en kwartaire afzettingen, Rep. Rijks Geologische Dienst, 85KAR02EX, Haarlem.